INVESTIGATION AND COMPARISON OF S700E STEEL GRADE WELDABILITY IN SHIPBUILDING

Numerical analysis on S700E steel grade

Lappeenranta–Lahti University of Technology LUT

Master's Programme in Mechanical Engineering, master's thesis

2024

Parisa Marivani

Examiners: Professor Timo Björk

Shahriar Afkhami, D.Sc. (Tech.)

ABSTRACT

Lappeenranta–Lahti University of Technology LUT

LUT School of Energy Systems

Mechanical Engineering

Parisa Marivani

Investigation and comparison of S700E steel grade weldability in shipbuilding (numerical analysis on S700E steel grade)

Master's thesis

2024

54 pages, 19 figures, 12 tables

Examiners: Professor Timo Björk and Shahriar Afkhami, D.Sc. (Tech.)

Keywords: High strength steels, S700E, welding configurations, welding pass, finite element analysis, thermal cycle, cooling rate, Simufact welding, shipbuilding

The numerical analysis provided valuable guidelines for improving welding practices and material selection in Shipbuilding. The aim of this research is to contribute to a deeper understanding of S700 steel's behaviour under some certain welding parameters, considering different working temperature with difference in number of passes. These considerations offer a pathway to enhance the performance, safety, and sustainability of marine vessels. In this regard, by utilizing simulation analysis this study explores how variations in the number of passes influence weldability of steel structures particularly S700E steel grade. In the following, temperature distribution, cooling rates, microstructural transformations within the weld zone, and the resulting microstructure within the heat-affected zone (HAZ) and fusion line are investigated. Moreover, results demonstrate the importance of optimising the number of welding passes in order to achieve desirable mechanical properties, such as toughness and ductility while reducing in phase transformations and residual stresses after welding process. The outcomes of this research are significant for the advancement of shipbuilding techniques, the application of high strength steels in heavy structures, particularly in the application of high-strength steels like S700. Consequently, by optimising the welding configuration, like the number of passes, under a specific welding process, shipbuilders can enhance the structural integrity and durability of marine structures, ensuring better performance in demanding environments.

ACKNOWLEDGEMENTS

Foremost, I would like to state my sincere gratitude to my supervisor Professor Timo Björk for his support and guidance throughout this study. His valuable assistance helped me in navigating the challenges of my research and his wisdom has inspired me appreciably. I would also like to express my appreciation to my second supervisor, Shahriar Afkhami for his high-priced wisdom throughout this journey. His thoughtful contributions have played a vital role in my academic development and the success of my thesis. Furthermore, I extend my heartfelt thanks to Hamidreza Rohani Raftar for his sincere support throughout the simulation process. His technical assistance and meticulous attention to detail were indispensable in achieving the objectives of my research.

I am also grateful to my family, friends, and peers for their endless encouragement and support, which has been a constant source of strength for me.

SYMBOLS AND ABBREVIATIONS

Roman characters

d	Thickness	[mm]
I	Current	[A]
Q	Heat Input	[kJ/mm]
T	Temperature	[ºC]
T_0	Working Temperature	[ºC]
$t_{8/5}$	Cooling time	[s]
t	time	[s]
V	Voltage	[V]

Greek characters

v	Travel Speed	[m/s]

Dimensionless quantities

F_2	Shape Factor
η	Thermal efficiency
Pcm	Cold cracking sensitivity index

Subscripts

8/5	800 ºC -500 ºC
0	Initial
wt%	Weight percent

Abbreviations

CCT	Continuous Cooling Transformation
CEN	Carbon Equivalent Number
CET	Equivalent Carbon Content
CEV	Carbon Equivalent Value
DQ	Direct Quenching
DQ+T	Direct Quenching and Tempering treatment
EEA	Eco-Efficiency Analysis
FEA	Finite Element Analysis
FEM	Finite Element Method
GMAW	Gas Metal Arc Welding
GTAW	Gas Tungsten Arc Welding
HAZ	Heat-Affected Zone
HSLA	High Strength Low Alloy
HT	Heat Treatment
LCSA	Life Cycle Sustainability Assessment
LW	Laser Welding
PA	Flat Position
QT	Quenching and Tempering
QT HSS	Quenched Tempered High Strength Steel
SAW	Submerged Arc Welding
SMAW	Shielded Metal Arc Welding
TMCP	Thermo-mechanical Controlled Process

Table of contents

Figures

Tables

1 Introduction

The use of novel types of high-strength steel (HSS) allows for less material utilisation while maintaining structural integrity. However, European rules for steel structural design now limit steel grade S700. To match HSS and Dual-Phase HSS behaviours with worldwide standards, we must first understand them better. This issue could lead to increased use of these steel varieties, lowering overall steel consumption in structures and machines while mitigating environmental concerns. (Neuvonen, R. & Peltoniemi, T. & Skriko, T. & Ghafouri, M. & Amraei, M. & Ahola, A. & Björk, T. 2023a, p. 6.)

Using high-strength, weldable construction steel materials is essential for creating slender and intricate structures. With their excellent strength-to-weight ratio, these materials provide notable advantages in terms of design weight, which reduces material consumption and increases cost-effectiveness. The minimisation of cross-sectional sizes is especially noticeable in sections that are influenced by stress. Additionally, by reducing the material requirements for supporting structures, the overall life cycle assessment of the structure will be improved. (Brätz, O. & Arnim, M. von & Eichler, S. & Gericke, A. & Hildebrand, J. & Bergmann, J.P. & Kuhlmann, U. & Henkel & K.M. 2023, p. 9.)

Through the improvement of steels capacity for sustainable building structures, high-strength steels with yield strength values of 700 MPa or more is the steel material that makes a building structure sustainable. Furthermore, the structural design takes advantage of the steel's broad elastic area to produce a pleasant and long-span space. As a result, future application growth is anticipated. (Kamo, T. & Ando, R. & Sasaki, M. & Suzuki, T. & Watanabe, Y. 2015, p. 1.)

Figure 1 shows a systematic overview of the fundamental aspects of sustainable structural engineering. According to (Kc & Gautam 2021, p. 456), it is necessary to present a full picture of how sustainable structural engineering integrates design, materials, and assessment methodologies in order to implement ecologically responsible construction techniques. They emphasise construction's environmental effects, particularly its water and carbon footprints, emphasising the importance of eco-friendly procedures. They also provide several methodologies for assessing the sustainability of construction projects, including the

Life Cycle Sustainability Assessment (LCSA), Eco-Efficiency Analysis (EEA), and Socio-Eco-Efficiency Balance (SEEbalance®), as well as other rating systems.

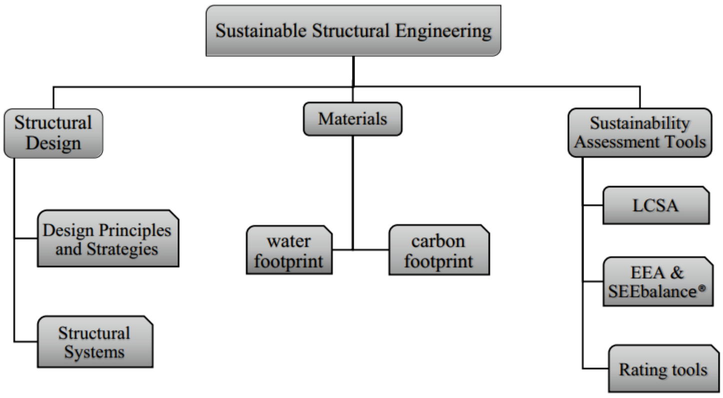

Figure 1. A framework for eco-friendly engineering: from design principles to sustainability assessment (Kc & Gautam 2021, p.10).

Additionally, in 2017, (Ban & Shi 2018, p.14), conducted a review of high-strength steel structures. In their research, they presented a comprehensive list of high-strength steel classes, all of which meet national specifications and have nominal yield strengths of at least 460 MPa (Figure 2).

National standard	HSS grade[a]	Quality class
EN 10025-6: 2004 (BSI, 2004a)	S460, S500, S550, S620, S690, S890, S960	Q, QL, QL1
ASTM A514/A514M-14 (ASTM, 2014)	A514/A514M (690 MPa)	—
ASTM A709/A709M-16 (ASTM, 2016)	HPS 70 W (485 MPa), HPS 100 W (690 MPa)	Zone 1, zone 2, zone 3
ASTM A913/A913M-15 (ASTM, 2015)	70 (485 MPa)	—
GB/T 1591-2008 (CNS, 2009)	Q460, Q500, Q550, Q620, Q690	C, D, E
GB/T 19879-2015 (CNS, 2015)	Q460GJ, Q500GJ, Q550GJ, Q620GJ, Q690GJ	C, D, E
JIS G 3106: 2015(E) (JSA, 2015)	SM570 (460 MPa)	—
JIS G 3128: 2009(E) (JSA, 2009)	SHY685	N, NS
JIS G 3140: 2011(E) (JSA, 2011)	SBHS500, SBHS700	—
KS D 5994: 2011 (KSA, 2011)	HSA800 (650 MPa)	—

Figure 2. Classification of high-strength steel (HSS) grades according to various national standards (Ban & Shi 2018).

Due to these material standards and the structural design guidelines, specific limitations are established for the material properties of HSSs. Research indicates that most design standards require structural steels to have a yield-to-tensile ratio of no more than 0.85 and an elongation percentage of at least 20% after fracture for plastic design purposes. However, most HSSs currently available in the market do not satisfy these criteria. Consequently, to enhance the mechanical properties of HSSs, advancements in metallurgy and production methods are still needed. Additionally, it is vital to establish reliable engineering design theories for HSS structures. (Ban & Shi 2018, p. 17.)

Research and development for naval steel is essential given the growing significance of marine transport in the global economy and the growing demands of globalization. The unique mechanical properties of shipbuilding steels distinguish them as one of the most essential materials used in the production of naval ships. In order to meet the demands of the harsh marine environment, these steels were specially designed to have higher strength, increased resistance to corrosion, and increased toughness. (Dias, J.M.S. & Santos Paes, L.E. dos & Santos, A.G.M. & Borba, T.M.D. & Paixão Carvalho, L. da & Vilarinho, L.O. 2023a, p. 3.)

1.1 Overview of the research objectives, problem, and questions

The thickness of HSSs and the requirement for metallurgical continuity to ensure the material's mechanical strength and toughness provide significant welding challenges in the shipbuilding industry. As a result, it's essential to comprehend every aspect of the welding procedure, how plate thickness affects welding parameters, and the final microstructure. (Dias et al. 2023a, p. 26.)

The importance of welding analysis in shipbuilding is highlighted by significant impact of welding process into alternation of material properties, which recognizing these affects is crucial for ensuring the structural integrity and functionality of shipping vessels. Particularly in the most northern Arctic locations, negative structural alterations in the HAZ have a unfavourable impact on the toughness and durability of welded joints. The integrity and usage of the welded structure depend on maintaining the required mechanical properties, such as toughness and ductility, as well as optimizing heat input during welding and controlling grain growth through microalloying. (Layus, P. & Kah, P. & Khlusova, E. & Orlov, V. 2018a, p. 76.)

In this regard, the aim of developing high-strength steels is to make a scientific understanding of plastic deformation in welded joints, along with the strategic use of microalloying and modifying elements in low-alloy and low-carbon steel’s structures. The development of the high strength low alloy (HSLA) family of steel has allowed for an improvement in the technology needed for forming welded joints, and its transformed microstructure is more suited for welding circumstances. (Chernyshov, E.A. & Romanov, A.D. & Romanova, E.A. 2016, p. 6.)

The main objective of the study is to compare and analyse the thermal behaviour of two welded joints of commercial S700E steel (as a commonly used HSLA steel and HSS), differing in the number of passes, within the context of shipbuilding, utilising specific welding parameters and a specific plate thickness. These welding conditions are designed to analyse the mechanical performance of the welded specimens under these set welding conditions. The results of this investigation are crucial to the shipbuilding industry, providing insights into how to use high-strength steels and to choose materials and welding practices for building durable and reliable vessels.

1.2 Framework

Table 1, and Figure 3, present an overview of the conceptual framework as well as a flowchart illustrating the procedure of this research, respectively.

Table 1. Conceptual framework of the study

<table>
<tr><th>Scope</th><th>Variable</th><th>Domain of influence</th><th colspan="2">Type of influence</th></tr>
<tr><td rowspan="2">Comparing the weldability of two S700E steel welded joints with different passes</td><td rowspan="2">Thermal behavior, working temperature, number of passes, welding parameters</td><td>Mechanical properties</td><td>Thermal cycle</td><td>Cooling rate</td></tr>
<tr><td>Microstructure</td><td colspan="2">Types of phases in different areas</td></tr>
</table>

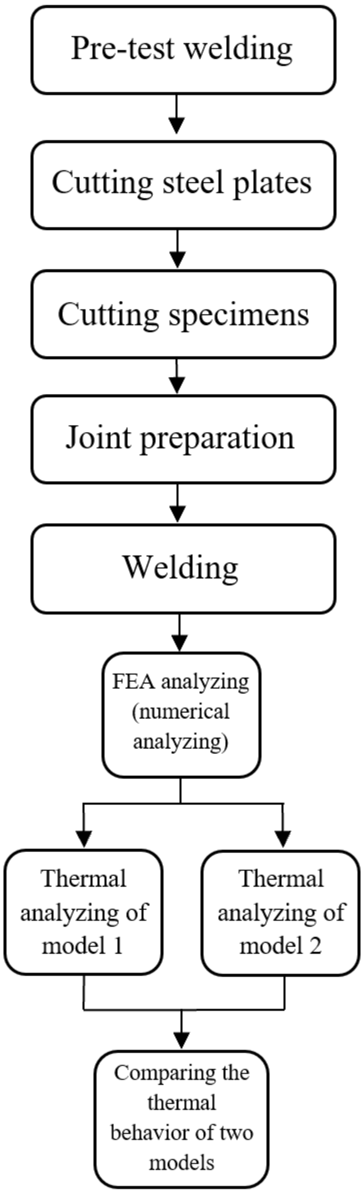

Figure 3. Progression of the research

2 Literature review

Over the past few years, a great deal of attention has been paid to the deployment of high-strength steels, specifically S700 steel, in shipbuilding applications, owing to the growing demand for lightweight but strong strength structures in the industry. As a result, shipping industry investigate in improving the performance and safety of the shipbuilding structures, while reducing overall weight. Therefore, weldability and strength evaluations of such materials have become critical. With an emphasis on the S700 steel specifically in the context of shipbuilding, this literature review provides a thorough analysis of recent findings and advancements on the weldability and strength properties of HSSs. The purpose of this review is to expand our knowledge of the detailed relationships between the properties of materials, welding techniques, and the quality of welded structures in naval applications.

2.1 High-strength steels

In recent years, HSSs have been known for their advantages in reducing the weight and dimensions of engineering projects, which results in fewer transportation challenges and less welding effort, thereby reducing overall engineering costs. Furthermore, by utilizing the lightweight structural engineering, the use of HSSs in engineering projects will maximize space efficiency and improve the strength and quality of constructions. In other words, due to the strong potential of HSSs in controlling the weld thickness while preserving the required strength, these materials are able in managing the durability and resource use, significantly boosting the overall integrity and efficiency of construction. (Jiang, J. & Wu, M. & Xu, T.T. & Bao, W. & Li, Z.H. 2024, p. 104.)

As a result, HSSs have been highly popular due to their ability to improve tensile strength and toughness, as well as their weldability exceeding standard levels. However, the selection of variables such as the material properties, welding parameters, welding process, pre-heating, post-weld heat treatment, carbon content, alternation in material microstructure, and chemical composition, affects the weldability of HSSs. Additionally, increasing steel yield strength has led to a strong focus on lightweight structures with satisfactory welding characteristics due to modern production processes developed recently. Moreover, reducing costs and, more importantly, reducing CO_2 emissions through the implementation of HSSs in structural engineering projects have resulted in the widespread use of HSSs as a proper and reasonable material. Despite this, since welded joints of HSSs have a lower deformation capacity comparing to the unwelded materials, they must withstand higher loads when steel strength increases, requiring careful selection of welding processes and material properties. (Ghimire, A. & Wald, F. & Vild, M. & Kabeláč, J. 2024, p. 54.)

In addition, complex multiphase microstructures of HSSs offer an adequate combination of strength and formability. Therefore, the modern thermomechanical treatment of steel, such as rolling, tempering, and quenching processes, are utilized in an innovative manner to enhance the capability of HSSs. In this regards, modern high-strength structural steels are known for their capability to improve mechanical properties, including strength and toughness. These qualities results from several factors, including the utilization of quenching and tempering (QT), the reduction of carbon content, and the proper selection of alloy elements. Thereby, to produce HSSs with the desired properties, direct quenching (DQ) has become a popular and economical method. Moreover, in the development of HSSs production, the combination of DQ and tempering treatment (DQ+T), now commonly known as quenching and tempering, is used to improve the material properties of HSSs, offering a complete solution for the production of modified steels. (Siltanen 2023, p. 6.)

In the following, there are significant developments in technologies used in shipbuilding steel production, focusing on the involvement of heat treatment (HT) of the thermo-mechanical control process (TMCP) type to enhance welding efficiency and address safety and sustainability concerns in the shipbuilding sector (Imai 2008.) Hence, in shipbuilding development, the advantages of utilizing the TMCP method to improve steel plate properties, eliminate the need for pre-heating, and enable high heat input welding are significantly remarkable. As a result, the increasing need for comprehensive studies in welding methods, along with their use in ship design and the properties of steel, cannot be disregarded. (Imai 2008.)

2.1.1 Shipbuilding steel plates

Nowadays, the improvement of mechanical properties in ship structures is in high demand, following recent advancements in shipbuilding, as these properties are key to ensuring the long-term reliability of ship structures, particularly in hazardous marine environments .(Luo, X.D. & Liu, H. & Zhu, Y.X. & Zheng, C.Y. 2014.) Moreover, ship plates are required to be durable, flexible, and fatigue-resistant to ensure safe navigation and durability, and to overcome the transportation challenges ships may face in extreme environmental conditions. Furthermore, the demand for lighter ships is rising due to environmental concerns and the need for more sustainable materials, which means ship steel plates must have even more rigidity and toughness. To meet these expectations, investigated studies are therefore concentrated on creating steel grades with high strengths and high toughness. (Wang, D. & Zhang, P. & Peng, X. & Yan, L. & Li, G. 2021, p 45.) As an alternative, one of the main goals for the shipping sector is to concentrate on reducing the weight or thickness of components without jeopardizing their durability. This effort intends to reduce emissions into the environment while reducing fuel usage and energy consumption (Hayat & Uzun 2011.) Consequently, one of the primary objectives in the marine industry is to develop and implement adequate heat treatment cycles that can alter the microstructure of shipbuilding steels. The objective of this method is to improve the mechanical characteristics of ship constructions, including strength, ductility, and toughness. (Luo et al. 2014.)

Finally, a range of steels with a yield strength of up to 690 MPa were developed in the 1980s. These steels perform exceptionally well in critical areas such as functionality, corrosion resistance, weldability, and low-temperature resistance. They allow welding in a variety of weather conditions without the need for preheating; in certain cases, they actually enable welding at below-zero temperatures This characteristic makes them more efficient for constructing large-scale welded structures in harsh environment. (Kupriyanova 2023, p. 88.)

2.1.2 S700E

High-strength structural steels like the Strenx 700E/F can achieve yield strengths of up to 700 MPa, depending on the thickness. Furthermore, Strenx 700 E/F fulfills EN10025-6 criteria for the S690 grade and thickness requirements. It is commonly used in applications requiring sturdy, load-bearing structures. Strenx 700E, which corresponds to S690QL, comes in plate thicknesses ranging from 4 to 160 mm. (SSAB 2019.)

Meanwhile, S690 is an HSLA steel extensively employed in structural settings. It is notably favoured for offshore applications, where it must maintain exceptional impact resistance, even in challenging cold conditions. In such scenarios, the steel typically possesses a predominantly bainitic microstructure. Additionally, its low carbon content enhances its weldability. To attain the desired mechanical properties, HSSs like S690 undergo a meticulous process involving forging followed by QT treatments. (Pezzato, L. & Gennari, C. & Chukin, D. & Toldo, M. & Sella, F. & Toniolo, M. & Zambon, A. & Brunelli, K. & Dabalà, M. 2020, p. 112.) The chemical composition and mechanical characteristics of S700E, as reported by its manufacturer, are described in Tables 1 and 2, respectively. (SSAB 2019).

Table 2. Chemical composition of S700E (SSAB 2019).

Steel Grade	C (max %)	Si (max %)	Mn (max %)	P (max %)	S (max %)	Cr (max %)	Cu (max %)	Ni (max %)	Mo (max %)	B (max%)
S700E	0.20	0.60	1.60	0.020	0.010	0.80	0.30	2.0	0.70	0.005
CEV= 0.49 CET= 0.32										

Table 3. Mechanical properties of S700E (SSAB 2019).

Thickness (mm)	Yield Strength (min MPa)	Tensile strength (MPa)	Elongation (min %)
4.0-53.0	700	780-930	14

2.2 Welding in shipbuilding

The welding of shipbuilding steels has been considered as a challenging process. The main reason is the required metallurgical continuity related to the mechanical strength and toughness of the material. Furthermore, due to the high thickness of the materials involved in shipbuilding structures, the selection of welding parameters often relies on the experimental methods. In this regard, shipbuilding sector requires a comprehensive understanding of the effects of thickness on the welding process. (Dias et al. 2023b.)

In addition, in shipbuilding, the structural integrity of low-alloy steel is compromised at high temperatures, necessitating advanced microalloying to prevent grain growth above 1100°C and ensure fusion boundary impact energy. Welding increases challenges, with heightened heat input causing grain growth and martensite formation due to low austenite stability. Reducing carbon content and alloying levels improves ductility but lowers HAZ toughness, and tempering further reduces toughness. Additionally, the combined effects of tempering and slow deformation induce residual stress impacts, leading to decreased plasticity and micro-crack formation at triple-grain junctions. This vulnerability to cracking at the weld line remains a concern, even with post-weld treatments. (Layus et al. 2018b, p. 9.)

Furthermore, distortions resulting from welding processes can adversely affect the design durability, mechanical stiffness, and visual finish of marine vessels, contributing to considerable ship construction costs. It is worth mentioning that the presence of distortions, which can occur even in the highest quality welds, is a separate issue from weld quality and does not necessarily indicate a flaw in the welding process. (Moore 2009, p. 5.)

As a result, the shipbuilding industry follows classification societies' high-quality standards, which ensure welder qualification and approved welding methods. Continuous monitoring ensures that these criteria are fulfilled. When weld defects are identified, they are typically repaired or removed; however, fitness-for-service assessments are employed to avoid inefficient repairs. Furthermore, fatigue improvement procedures are utilised to prevent or fix fatigue-related defects at welds, increasing the ship's durability. (Moore 2009., p. 10.)

2.2.1 Weldability of HSSs

The weldability of HSSs can be problematic due to the effects of welding on the HAZ. Laser and hybrid laser-arc welding can soften the HAZ, not as much as submerged arc welding and gas metal arc welding, resulting in tempered martensite and lower tensile strength, while also causing hardening in certain cases. Therefore, understanding and regulating these effects is critical to the integrity and performance of welded high-strength steel joints. (Rudskoi & Parshin 2021, p. 33.)

Additionally, when welding HSSs, regardless of the welding method or alloy, several critical issues frequently occur, such as cracking and softening in the HAZ, along with inadequate toughness and ductility. These issues are commonly attributed to the lack of sufficient control over the heat input and the rate of cooling in the welding process, the chemical composition of the steel preventing the creation of large grain structures, and a logical compromise between ductile and brittle elements in the microstructure of the HAZ and the welded joint. (Tasalloti, Kah & Martikainen 2017, p. 225).

S700 steel, known for its low carbon equivalent (CEV), is generally recognised for its excellent weldability, negating the requirement for pre-heating. (Skowronska, B. & Chmielewski, T. & Golanski, D. & Szulc, J. 2020, p. 99.) However, if pre-heating needs to be conducted, it typically occurs due to the filler wire's weldability or to minimise hydrogen content in the weld. In such situations, the pre-heating temperature should be below 100 °C. (Górka 2015, p. 3).

2.2.2 Hardenability and weldability

Most weldability issues associated with quenched and tempered high-strength steels arise from the undesirable modification of the original fine-grained microstructure. Some zones become softer or harder within the HAZ. In the case of structural steels, the coarse-grained zone within the HAZ provides the biggest threat to toughness. In other words, in high-strength steel welding, the HAZ is critical because it is where heat causes the steel to change phase partially. This issue can alter the carbon content, which can affect the steel's strength and hardness. Additionally, this zone is particularly challenging in QT or DQ steels, leading to cracking and reduced toughness, similar to issues in the coarse-grained zone that impact the steel's fracture resistance. (Gáspár 2019. p. 1.)

As an example, in the study conducted by (Shahriar Afkhami 2018, p. 7), the assessment of the hardenability and weldability of low-carbon steels is determined through the calculation of the Carbon Equivalent Number (CEN) using equation shown below. According to the study, steels with a CEN of less than 0.45% have the potential to exhibit improved weldability properties.

$$CEN = \mathrm{C_{wt\%}} + 0.5\left(\frac{\mathrm{Si_{wt\%}}}{24} + \frac{\mathrm{Mn_{wt\%}}}{6} + \frac{\mathrm{Cu_{wt\%}}}{15} + \frac{\mathrm{Ni_{wt\%}}}{20} + \frac{\mathrm{Cr_{wt\%}} + \mathrm{Mo_{wt\%}} + \mathrm{Nb_{wt\%}} + \mathrm{V_{wt\%}}}{5} + 5\mathrm{B_{wt\%}}\right) \tag{1}$$

2.2.3 Cold cracking in HSSs

Cold cracking in HSSs results from welding residual stresses, heat-induced microstructural changes, and hydrogen penetration, while rapid heating and cooling cycles during welding can alter the microstructure of the material, leading to increased hardness and decreased ductility. Consequently, the material is more likely to crack when subjected to tensile stresses. In other words, the heat produced in the welding process affects the structure of the steel, resulting in it being less ductile and more susceptible to cracking. Furthermore, cracks can form in steel materials due to the presence of hydrogen or moisture in welding materials. Despite this, cracks may not appear immediately, but instead develop gradually over time as the steel cools down and hydrogen diffuses. (Schroepfer et al. 2024.) Figure 4 demonstrates how brittle microstructures, high tensile stress, and elevated levels of diffusible hydrogen contribute to cold cracking in HSSs. (Hopf, A. & Klug, M. & Durmaz, K. & Goth, K. & Jüttner, S. 2023, p. 9.)

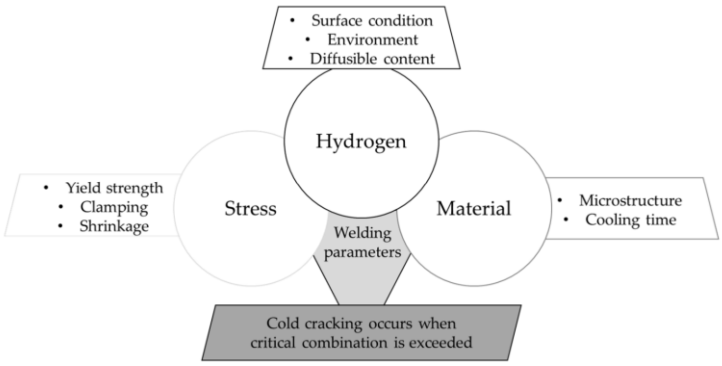

Figure 4. The main factors influencing the possibility of cold cracking (Hopf et al. 2023, p 9).

The hydrogen-crack test results demonstrate that reducing diffusible hydrogen levels effectively lowers the susceptibility of cold cracking. Since only bending forces are applied to the test specimens, any observed failures could be attributed to hydrogen-induced cold cracking. (Klett & Hassel 2020, p. 78.)

In this context, (Sampath 2021), utilizes the cold cracking sensitivity index (P_{cm}) parameter to evaluate the weldability and susceptibility to cold cracking of the HSSs material. The investigation shows that higher P_{cm} values suggest higher hardenability, which can lead to increased toughness while also creating more brittle microstructures. Additionally, to reduce the risk of cold cracking during welding, it is suggested to control the carbon content below 0.10 wt%. Therefore, evaluating the carbon equivalent number (CEN) can be an acceptable factor to assess the risk of cold cracking in HSSs, particularly in high strength steel like S700MC with niobium levels exceeding 0.04 wt%. Figure below demonstrate the susceptibility of cold cracking in HSSs in different zones. (Shahriar Afkhami 2018, p. 7.)

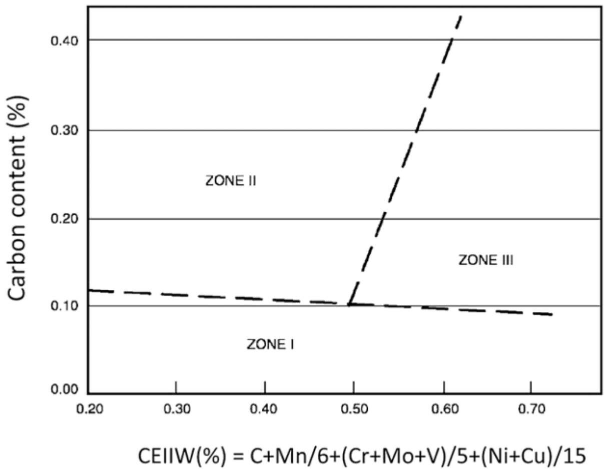

Figure 5. The susceptibility of steel to HAZ cold cracking, influenced by CEN: Zone I demonstrates good weldability, Zone II requires careful observation during welding, and Zone III is challenging in terms of welding (Shahriar Afkhami 2018, p. 7).

2.2.4 Pre-heat temperature, interpass temperature, and the critical cooling time

The cooling time, denoted as $t_{8/5}$, is the period required for a weld pass and its HAZ to cool from 800 °C to 500 °C (Figure 6). This parameter significantly impacts the microstructure of the weld joint. It can also be utilized to evaluate the influence of reheating on the microstructure formed during the initial cooling phase. Microstructural transformations occur within the temperature range of 800 °C to 500 °C. The resulting microstructure, which can be ferritic, pearlitic, bainitic, or martensitic, depends on the duration of $t_{8/5}$. Prolonged $t_{8/5}$ cooling times may result in the formation of only ferrite and pearlite from the austenite. (Celin, Bernetič & Balantič 2014.)

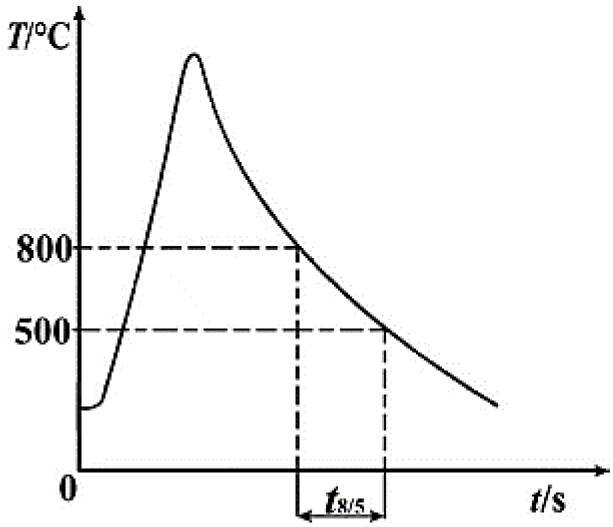

Figure 6. Demonstrated cooling time graph (with $t_{8/5}$) in welded joints (Celin et al. 2014, p. 108).

In the following, CEV, as an examined value, can also be considered to determine the critical cooling time, the required pre-heat temperature in welding process, and to predict the potential risk of cold cracking during the welding process (Klett & Hassel 2020). Additionally, CEV and CET values control various parameters such as pre-heat and interpass temperature, with higher CEV or CET values resulting in increased pre-heat and interpass temperatures. (Shahriar Afkhami 2018, p. 5.) On the other hand, despite the properties of the utilized welding filler, the required minimum pre-heat temperature for welding joints effectively remains consistent while dealing with materials with yield strengths up to 690 MPa. This issue is attributed to the CET of the base metal, which generally increases the carbon content of the welded metal by at least 0.03%. However, for consumables with yield strengths higher than 690 MPa, it is vital to consider the minimum pre-heat temperatures of both consumable and the HSS. The reason for this issue is that the CET of the filler material can significantly differ from the CET of the HSS, such as Strenx steels. In such cases, it is suggested to select the higher pre-heat temperatures. (SSAB 2024.)

2.3 Welding process for joining HSSs

During the welding process of quenched and tempered high-strength steels (QT HSS), it is critical to carefully determine the material properties to keep the integrity and durability of the welded structure. Moreover, the chemical composition of the HSSs and the welding techniques can alter the microstructure and more importantly affect the mechanical properties of the welded joints, consequently these factors significantly affect the weldability of the HSS materials. As a result, to minimize the reduced toughness and the risk of cold cracking, it is crucial to specify the proper filler materials, welding conditions, and post-weld heat treatments in the welding process. Identifying the challenges associated with welding HSSs and considering suitable welding techniques can reduce the cost and effort required to meet the satisfactory welded joints. (Weglowski, M. St 2018, p. 1.) Additionally, (Węgrzyn et al. 2023), state that to obtain the satisfactory welded joints which are capable of enduring cyclic loading and ensuring the required durability and ductility, several crucial steps are required to be considered. These steps include implementing pre-heating measures, utilizing gas mixtures with lower oxidation potential, and considering electrode fillers with reduced carbon content.

The welding methods utilized in welding of HSSs include Submerged Arc Welding (SAW), Gas Tungsten Arc Welding (GTAW), Shielded Metal Arc Welding (SMAW), Gas Metal Arc Welding (GMAW), and Laser Welding (LW). (Shahriar Afkhami 2018, p. 8.) However, according to the existing research sources, the most popular welding process utilized for welding HSSs are GMAW and LW. (Ghafouri et al. 2022, p. 7.) Accordingly, the heat input of arc welding methods often leads to slow cooling rates, resulting in softening of the HAZ and reducing the material and welding strength. In contrast, LW offers significant advantages, including deep penetration resulting in a more suitable HAZ, as well as a reduction in heat input, leading to lower residual stresses and thermal distortions. (Guo et al. 2017, p. 67.) On the other hand, LW offers higher cooling rates, which may result in the formation of additional martensite. Therefore, it is crucial to utilize suitable welding techniques, ensuring the implementation of high-quality welded joints. (Węglowski et al. 2017, p. 9.)

2.4 Welding parameters

The selection of welding parameters, including welding current (I), arc voltage (V), speed (v), cooling time (i.e., $t_{8/5}$), and specific heat input, are the key factors in welding process of HSSs to ensure the high-quality welded joints. Additionally, considering the base and filler materials, weld design, welding equipment, and the skill level of the welder are all additional factors that potentially affect the welding quality results. Low heat input can increase the strength and hardness of the welded material, but it may also lead to a higher risk of cold cracking. Conversely, high heat input could create a coarsely grained microstructure, thereby weakening the weld joint. (Celin et al. 2014.)

For instance, (Chiew, S.P. & Cheng, C. & Zhao, M.S. & Lee, C.K. & Fung, T.C. 2019, p. 2), investigate and outline the welding parameters influencing the final quality of welded joints, including a fixed voltage of 30 V for all joints, a specific plate thickness, electrode diameters of 3.2 mm, 4.0 mm, and 5.0 mm, and various currents adjusted for each electrode size, demonstrated in Table 4. These parameters result in different average welding heat inputs of 1.14 kJ/mm, 1.60 kJ/mm, and 1.74 kJ/mm, respectively. The results demonstrate that higher heat inputs influence the weld's microstructure and mechanical properties by extending the cooling time, which are driven by $t_{8/5}$ values of 12.6, 22.6, and 26.0 seconds, respectively.

Table 4. Welding parameters examined in the study (Chiew et al. 2019, p. 3).

Joint	Electrode diameter (mm)	Voltage (V)	Current (A)	Average welding heat input (kJ/mm)	$t_{8/5}$
BJ16-3.2	3.2	30	117	1.14	12.6
BJ16-4.0	4.0	30	125	1.60	22.6
BJ16-5.0	5.0	30	160	1.74	26.0

2.4.1 Joint design

In the field of welding, joint design and implementation are critical for achieving the highest levels of durability and strength in welded structures. Variations in mechanical properties like strength and ductility can result from differences in the microscopic structure of the component at the weld joint caused by different welding methods. In more straightforward terms, the type of arc welding method, GMAW for instant, can affect how metal grains and phases, such as ferrite and pearlite, are spaced and instructed in the weld region. Stated differently, every form of joint has distinct properties and is employed in welding, which can be influenced by the welding technique selected. (Shekhar, S. & Rai, P. & Ayub, A. & Mata Vaishno, S. & Srivastava, A. & Sekhar, S. & Nema, A. & Pandey, A. & Jha, R. 2016,

p. 35.) While most studies only look at specific welding parameters and joint types or welding processes, (Neuvonen et al. 2023a, p. 8), emphasize the importance of joint type and design in the welding of HSSs, focusing on the effects of HAZ and geometric constraints on the ultimate load-carrying capacity of welded joints. According to this study, joint geometry should be taken into account in addition to restricting HAZ. Designing weldments with rigorous geometric limitations can manage the susceptibility to softening of DQ HSSs while fully exploiting the base material's capacity.

The experimental study on the welding effects on S690Q high-strength steel butt joints reveals several critical insights into the changes in microstructure, hardness, and tensile properties due to welding. Welding transforms the primary microstructure from tempered martensite to granular bainite in the coarse-grained HAZ and to a mix of ferrite and cementite in the fine-grained HAZ, with some tempered martensite decomposing to ferrite in the tempering zone. In this regard, micro-hardness testing demonstrates that this transformation results in the creation of a softer layer within the HAZ, and that the width of this layer develops with increasing welding heat inputs. Moreover, tensile studies indicate that when welding heat input rises, the butt joints' yield and tensile strength diminish, and fractures generally occur in the heat-affected zone. Furthermore, after welding, the butt joints become less ductile due to localized plasticity in the heat-affected zone and a significant amount of plastic stress, which might cause an earlier fracture under tensile stress. (Neuvonen et al. 2023b, p. 9.) However, there are factors beyond joint type that influence the effectiveness of welding HSSs, particularly with a focus on S690Q grade steel, (Chiew et al. 2019, p.14), investigate the impact of welding on the mechanical properties of butt joints in HSS structures and concludes that welding heat input is a critical factor affecting the durability of HSS butt joints. Elevated welding heat inputs result in significant microstructural changes in the HAZ, enlarging the softened layer and affecting mechanical properties such as yield and tensile strength, as well as the ductility of welded joints.

3 Numerical analysis procedure

This chapter provides a numerical analysis of two models of Strenx 700E steel grade welded joint, differing in number of passes, focusing on investigating the development of welded joint capabilities caused by various welding parameters and pass numbers. In the previous chapter, the chemical compositions and mechanical properties of the S700E steel grade are provided in Tables 2 and 3, Section 2.1.3. Plate thickness is a crucial factor influencing the performance of welded joints in different HSSs grades, which particularly highlighted in this study.

In this study, two different welding configurations are considered for finite element analysis (FEA). Notably, in both models, the plate thickness is equivalent. Additionally, the pre-test welding data gathered prior to the investigation is utilized for the welding parameters of finite element analysis. With this method, we can precisely evaluate the efficacy of the welding processes under determined circumstances. The initial focus of this investigation is on a plate thickness of 15 mm, which is widely used in many structural applications and offers a compromise contribution between welding process and joint performance. Nevertheless, it is considered that to fully comprehend the welding parameters effect, a wider range of thickness values could be put into investigated in the future. Therefore, it is suggested that future tests could include plates as thin as 6 mm and as thick as 20 mm to explore a broader range of potential outcomes based on plate thickness variations.

3.1 Joint preparation and groove type

The joint preparation and groove types used for S700E steel grade are carefully selected to optimize the welding process and achieve maximum performance. The study focuses on butt welds using Y-groove joints, which are designed to meet the specific requirements of SAW, the chosen welding technique for its suitability to thicker materials and its efficiency in producing high-quality welds.

The preparation of the Y-groove follows the standards set by EN9692-2, ensuring consistent quality and compliance with international welding standards. In particular, the Y-groove joint configuration is preferred because it facilitates simpler access and control, reduces the possibility of inaccuracies and improves the overall quality and durability of the weld. In addition to guaranteeing strong welds and deep penetration, it facilitates the welding process. Additionally, this particular type of groove makes it easier to regulate the heat input and cooling speed, two critical processes for preserving the intended mechanical qualities of the weld. The maximum number of welds passes that can be applied depends on the type of weld joint, which in turn affects the weld's rate of cooling. Groove types and joint angles are presented in Figure 7. Additionally, to preserve structural integrity and manage temperature input, welding testing suggests a pass range of three to five in finite element analysis.

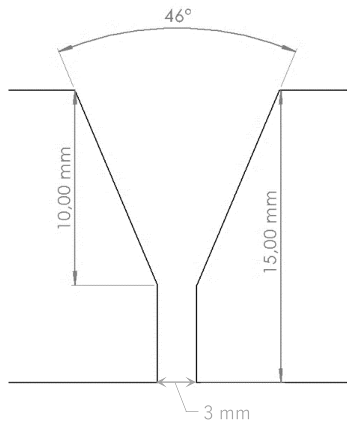

Figure 7. Schematic of weld groove

3.2 Welding process

The welding is primarily carried out via SAW with careful preparation to minimize angular distortions. The SAW welding process is utilized because it is effective when working with thick materials and offers deep penetration, high-quality welds. This provides it a perfect approach for high-strength steel grades, especially S700 HSS. It is particularly suitable for our analysis objectives since it allows precise control of heat inputs and working temperatures, which plays a vital role in influencing the microstructure and mechanical properties of the welds.

In this preliminary phase, Strenx 700E steel grade subjected to different numbers of welding passes is investigated. Specifically, we analyzed models with five passes (model 1) and three passes (model 2), both conducted at specified working temperatures. The simulation analyses of these models were performed and will be utilized for further comparison with experimental data. The diagrams for model 1 and model 2 are shown in Figures 8 and 9, respectively.

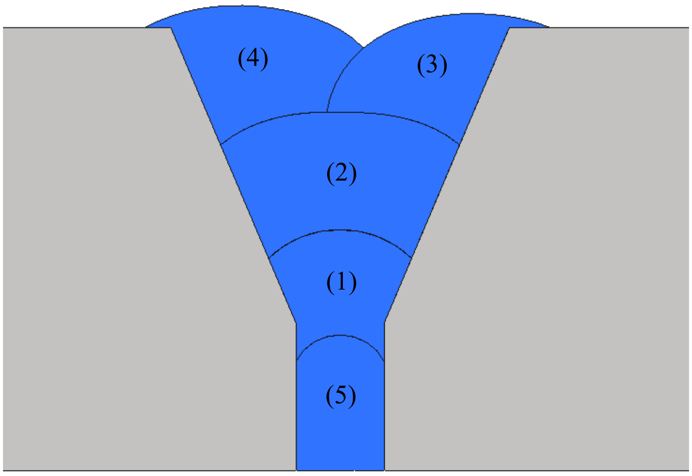

Figure 8. The schematic of five passes in model 1

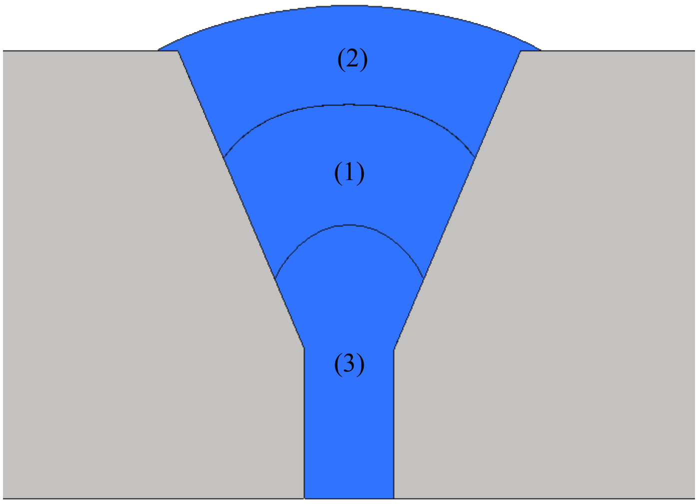

Figure 9. The schematic of three passes in model 2

Moreover, it is crucial that the optimal joint preparation minimizes axial misalignment and angular distortion. This is because such imperfections can significantly affect the strength and integrity of the welded joint.

3.2.1 Plate dimensions and specimen

Following joint preparation and welding trials, the Y groove joint is welded onto a 1000×920 mm plate. From that plate, individual specimens are then processed for simulation. It is also important that the specimen preparation (cutting) should not influence the results. The sheet cut to pre-shape, as shown in Figure 10, minimizes the effect. Figure 10 provides a detailed illustration of the exact dimensions of the plate used in the study.

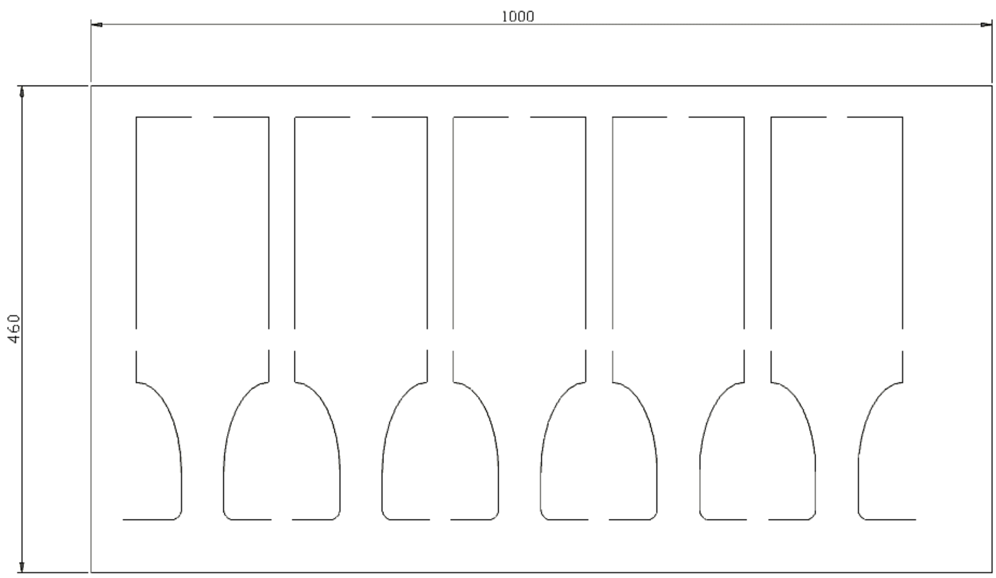

Figure 10. Schematic view of welded plate

It is worth mentioning that no mixed or dissimilar joints were tested or analyzed in this preliminary investigation.

3.2.2 Welding parameters

As mentioned before, SAW was employed in a flat (PA) welding position, following the parameters outlined in Tables 5 and 6, for model 1 and model 2, respectively. The investigation focused on butt joints welded at room temperature. Additionally, a 4 mm filler wire was selected based on the shipyard's specifications.

Table 5. Parameters for SAW considered for model 1

Welding Current (A)	Arc Voltage (V)	Travel Speed (mm/min)	Wire Size (mm)	Interpass Temperature (ºC)
480 – 550	26.5 – 28	550 – 580	4 mm	33 – 90
Polarity	Heat Input (kJ/mm)	Consumable	Welding position	Working Temperature (ºC)
DC+	1.39 – 1.59	ESAB OK Autrod 13.43 + ESAB OK Flux 10.62	PA	20

Table 6. Parameters for SAW considered for model 2

Welding Current (A)	Arc Voltage (V)	Travel Speed (mm/min)	Wire Size (mm)	Interpass Temperature (ºC)
600 – 750	27 – 32	540 – 590	4 mm	86 – 109
Polarity	Heat Input (kJ/mm)	Consumable	Welding position	Working Temperature (ºC)
DC+	1.71 – 2.33	ESAB OK Autrod 13.43 + ESAB OK Flux 10.62	PA	21

3.3 Numerical simulation

In the numerical study using Simufact welding software, the FEA of S700E steel plates welded with a Y-groove joint was comprehensively examined. The aim is to investigate the thermal and mechanical properties of the joints under different numbers of welding passes and operating temperatures, focusing on two specific types.

3.3.1 Numerical analysis requirements

Throughout the numerical process, a number of data points need to be considered in order to ensure that the model is accurate. In this regard, data from pre-test welding was acquired and then used to analyse the welding process numerically.

A suitable specimen was chosen, featuring a Y-groove joint designed with one bevelled and one straight edge, creating the essential Y shape for the welding process. The geometry was meticulously defined to mirror the joint configuration used in real-world welding.

The finite element mesh for the specimen and welding passes was created using Apex software. To ensure precise capture of thermal gradients and mechanical stresses, a finer mesh, 0.5 mm in the welded line with a spacing of 10 mm, was applied to the weld zone. In contrast, areas further from the weld were given a coarser mesh (1 mm) to strike a balance between computational efficiency and accuracy. The mesh consisted of 3D solid elements, which were suitable for both the base plates and the weld material, as shown in Figures 11, 12.

Material properties for S700E steel were defined, and welding parameters were established using Goldak's double ellipsoid model for the heat source, which, by adjusting the model parameters, closely simulates the actual heat input from the submerged arc welding process. Additionally, the welding speed, current, voltage, and power input were set based on pre-test welding data, ensuring the simulation accurately reflected real-world conditions.

Appropriate boundary conditions were then established to match the real-world welding process and achieve accurate results. These conditions were applied to prevent any rigid body motion during the simulation. This prevention involved fixing one end of the plate to stabilise the model and using a working plate suitable for back welding. Additionally, initial temperatures were set at 20 °C for model 1 and 21 °C for model 2, reflecting slight variations in working conditions.

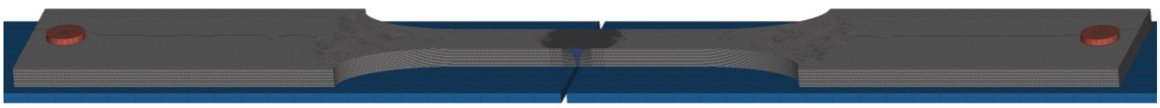

Figure 11. The 3D view of the solid meshed of model 1 considering proper mechanical conditions

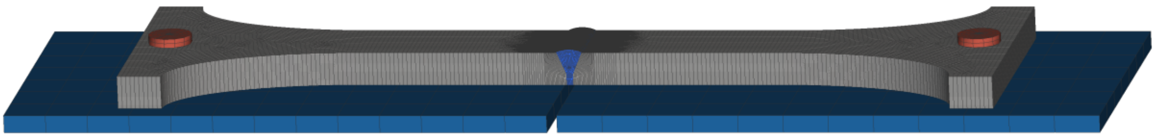

Figure 12. The 3D view of the solid meshed of model 2 considering proper mechanical conditions

It is also worth mentioning that due to the high volume of calculations during numerical analysis, influenced by the mesh size, and in order to minimise the calculation duration, the length of the specimen for model 2 has been reduced while maintaining excellent mesh accuracy (Figure 12).

3.3.2 Cooling time

In FEA, using Simufact software to evaluate the weldability of steel grade plates, calculating the cooling time $t_{8/5}$ is crucial for accurately simulating and analysing thermal cycles during welding. The $t_{8/5}$ cooling time, which measures how long it takes for the weld to cool from 800 °C to 500 °C, is directly related to the formation of microstructures in the HAZ and weld metal. These microstructures significantly impact the mechanical properties of the welded joint, such as hardness, strength, and toughness. By calculating $t_{8/5}$, we can predict the resulting microstructures and their distribution, assess the potential for weld defects like cracking, and evaluate the effects of various welding parameters and techniques. In addition, two-dimensional heat dissipation occurs during the welding of a relatively thin plate. (Shahriar Afkhami 2018, p. 8.)

$$t_{8/5}=(4300\text{-}4.3\mathrm{T}_0)\times10^5\times\left(\frac{Q}{t}\right)^2\times\left(\frac{1}{(500\text{-}\mathrm{T}_0)^2}-\frac{1}{(800\text{-}\mathrm{T}_0)^2}\right)\times\mathrm{F}_2 \quad (2)$$

According to equation 2, the cooling time for two-dimensional heat dissipation grows with the square of the energy per unit length and the pre-heating temperature but decreases with the square of the workpiece thickness.

Where T_0 is working temperature [ºC], d is thickness [mm], Q is welding heat input [kJ/mm], and F_2 is a dimensionless shape factor, which is defined according to Table 7.

According to (Shahriar Afkhami 2018, p. 8.), the following formula in bellow is utilized to determine the heat input Q:

$$Q = \eta \times \frac{(V \times I)}{v} \tag{3}$$

Where η shows thermal efficiency according to Table 8, V is the voltage [V], I demonstrate current [A], and finally, v is the welding speed [m/s].

Table 7. Shape factors according to joint configuration (Shahriar Afkhami 2018, p. 6)

Type of weld		Shape factor F_2
Name	Schematic view	
Bead on plate		1.00
Between runs, butt weld		0.90
Single run, Fillet weld on a corner	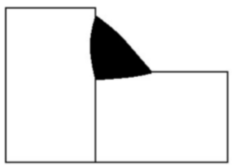	0.67 – 0.90
Single run, fillet weld in a T-joint	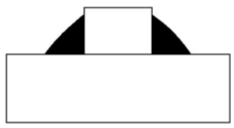	0.45 – 0.67

Table 8. Thermal efficiency according to the welding process (Shahriar Afkhami 2018, p. 7)

Type of welding process	Thermal efficiency (η)
Submerged arc welding	1.0
Manual metal-arc welding	0.8
Metal-inert gas welding	0.8
Metal-active gas welding	0.8
Self-shielded tubular-cored arc welding	0.8
Self-shielded tubular-cored arc welding with active gas	0.8
Self-shielded tubular-cored arc welding with inert gas	0.8
Tungsten-inert gas welding	0.6
Plasma arc welding	0.6

As a result, Tables 9 and 10 show the calculated $t_{8/5}$ for each pass of Model 1 and Model 2 respectively. It is important to mention that average welding parameter values (voltage, welding speed, and current) are considered for each model in this study. Furthermore, for both models, the average interpass of 60° is considered starting with the second pass. According to equation 2, this assumption ensures the uniform heat input, which leads to graduate cooling times for each pass in each model.

Table 9. Calculated cooling time in model 1

Model 1- Five passes											
Base material	Heat input (kJ/mm)	Pass No.1		Pass No.2		Pass No.3		Pass No.4		Pass No.5	
		$t_{8/5}$	T_0	$t_{8/5}$	T_0	$t_{8/5}$	T_0	$t_{8/5}$	T_0	$t_{8/5}$	T_0
S700E	1.43	9.34	20°	11.08	60°	11.08	60°	11.08	60°	11.08	60°

Table 10. Calculated cooling time in model 2

Model 2- Three passes							
Base material	Heat input (kJ/mm)	Pass No.1		Pass No.2		Pass No.3	
		$t_{8/5}$	T_0	$t_{8/5}$	T_0	$t_{8/5}$	T_0
S700E	1.944	17.24	21°	20.37	60°	20.37	60°

4 Results and discussion

The principal objective of this study is to provide an analysis and comparison of two various types of welded joints, the first model experience five passes and the second model three passes, under different working temperatures. The study examines the temperature distribution, cooling rates, and thermal gradients generating throughout the welding process using proper FEA thermal simulations. Comprehending of these graphs is essential to investigating the mechanical properties and following microstructural alternation of the welded material. Through welding process simulation, it is demonstrated that the working temperatures impact the heat cycles experienced by the welded joints and the HAZ.

The chapter proceeds with a detailed examination of the heat profiles produced by the welding process and the heat input. Additionally, the highest temperatures obtained in various zones of the weld metal, as well as the cooling rate throughout the three regions of both models, are demonstrated. Moreover, the development of different microstructural phases for both models is highlighted specially in the critical temperature range of 800 °C to 500 °C. In the following, this study also highlights how the extra passes impact the overall temperature gradient of the welded joints and explains the variations in thermal behaviour between these two configurations.

4.1 Peak temperature analysis

IN this section, for each welding configuration, the fusion line, HAZ, and base metal are the three different areas within the welded joints that are the focus of the peak temperature analysis. In each model, the cross-section at the midpoint is considered to maintain accurate and consistent analysis. The highest temperature value of each region generated throughout the welding process have been evaluated. This analysis highlights the impact of various welding passes and working temperatures within the S700E HSS, offering crucial insights into the thermal behaviour of the weld metal. More importantly, these profiles offer a strong comprehending of mechanical and microstructural characteristics of the welded joints. In ultimately, these findings could potentially implement to improve HSS welding in shipbuilding applications.

4.1.1 Thermal behaviour analysis of welded regions in model 1

The thermal analysis of model 1, shown in Figure 13, consisting of four faces and a single back weld, investigates the peak temperature behaviour in three critical regions: the fusion line, the HAZ, and the base metal. This analysis relies on temperature profiles observed across five welding passes, each followed by a 100 s cooling interval to reach the 82-90 ºC interpass temperature which was determined during preliminary welding tests. Figure 13 demonstrates how these regions respond to welding and cooling cycles.

In the first pass, the fusion line heats up rapidly to a high temperature and then cools down sharply from its peak temperature within the first 40 seconds, entering a more gradual cooling phase. The HAZ also experiences a rapid temperature increase but not as high as the fusion line, followed by a slower cooling rate. Out of the three zones, the base metal cools and heats up less quickly since it is farthest away from the direct heat source. The fusion line has cooled considerably after 40 seconds, and the rate of temperature decline is now decreasing. Additionally, after its first sharp decrease, the HAZ is still cooling steadily. Furthermore, the base metal cools as well, but much more slowly and with a more progressive drop in temperature. Following this, the three areas cool more uniformly and at comparable temperatures.

The fusion line heats extremely rapidly during the second pass as well, peaking at temperatures comparable to the temperatures of the first. The HAZ and base metal, however, begin at a higher a starting point temperature because of the heat that persisted after the first pass. In addition to the accumulated heat, the heating and cooling rates during the second pass are comparatively slower. While the three regions eventually reach similar temperatures in this pass, it takes longer compared to the first pass. In the third pass, the pattern continues with the fusion line heating and cooling rapidly; however, the cooling rates in these regions are almost slower, indicating that the material is retaining more heat with each subsequent pass. As a result, the three regions now take even longer to reach similar temperatures and cool down uniformly. In the fourth pass, the temperatures in all three regions increase slightly due to the accumulated heat from the earlier passes. However, during the fifth pass, which functions as the back weld, even though the fusion line experiences a significant peak in temperature due to the direct application of the heat source, the other regions show lower temperatures.

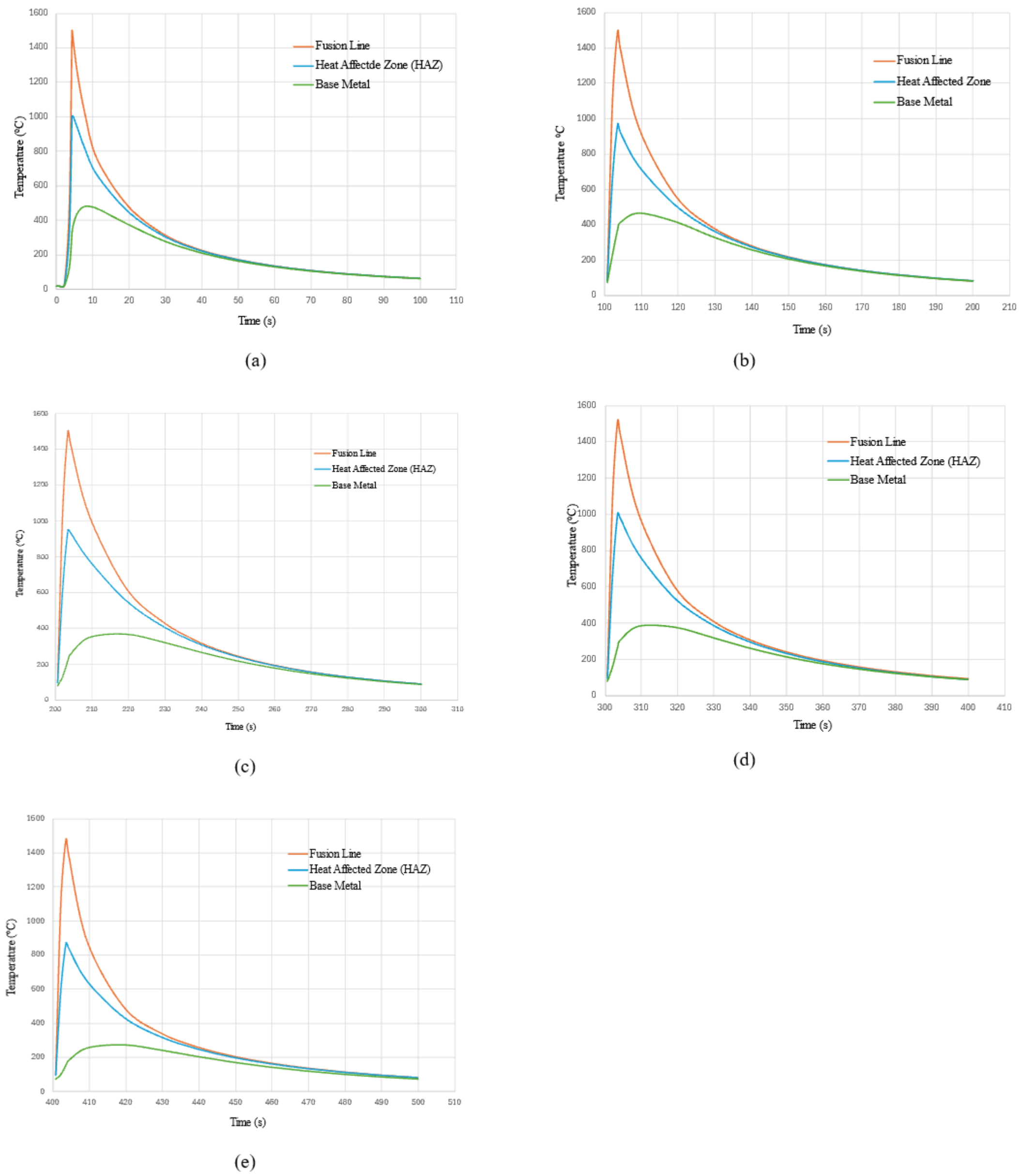

Figure 13. Temperature profiles of five passes of model one in the SAW process, [Graphs from (a to e) are shown the temperature profile for (the first, second, third, fourth, and fifth passes, respectively)]

Figure 14 presents a zoomed-in view of the temperature profiles for five passes in the following section. This figure highlights the maximum temperature values in the graph to provide a deeper analysis. In the first pass, the fusion line reaches the highest peak at 1502 °C, with HAZ peaking at 1007 °C, and the base metal at 481 °C. Moving to the second pass, the fusion line shows a slightly lower peak of 1497 °C, HAZ peaks at 969 °C, and the base metal at 464 °C. The third pass maintains a similar tendency with the fusion line at 1496 °C, HAZ at 947 °C, and base metal at 366 °C. In the fourth pass, the fusion line peaks at 1516 °C, the highest among all passes, with the HAZ matching the first pass at 1003 °C, and the base metal slightly higher at 383 °C. Finally, the fifth pass or back weld shows the fusion line at 1480 °C, HAZ at 870 °C, and the lowest base metal peak at 272 °C. Subsequently, the data shows that the fusion line consistently exhibits the highest temperatures, with slight variations around 1500 °C, peaking at similar times for each pass. The peak temperatures for the fusion line occur at 4 s (first pass), 104 s (second pass), 204 s (third pass), 304 s (fourth pass), and 404 s (fifth pass). These consistent peak times indicate a rapid and uniform heat input across all passes. The HAZ temperatures gradually decrease from the first to the fifth pass, peaking simultaneously with the fusion line at each respective time point. This simultaneous peaking suggests efficient heat transfer from the fusion line to the HAZ. The peak times for the HAZ are 4 s (first pass), 104 s (second pass), 204 s (third pass), 304 s (fourth pass), and 404 s (fifth pass).Base metal shows a clear trend of decreasing peak temperatures, with the peaks occurring progressively later than those of the fusion line and HAZ. Base metal peaks at 8 s (first pass), 109 s (second pass), 219 s (third pass), 309 s (fourth pass), and 419 s (fifth pass). This delay in peak times for the base metal reflects cumulative heat effects and the gradual distribution of heat away from the weld area, indicating heat accumulation effects that the base metal heats up more slowly and retains heat for a longer duration. All the information from Figure 14 is listed in Table 11.

Table 11. Data gathered from temperature-time graphs of model 1

Number of Passes	Fusion line		HAZ		Base Metal	
	Time (s)	Temperature(ºC)	Time (s)	Temperature(ºC)	Time (s)	Temperature(ºC)
NO.1	4	1502	4	1007	8	481
NO.2	104	1497	104	969	109	464
NO.3	204	1496	204	947	219	366
NO.4	304	1516	304	1003	309	383
NO.5	404	1480	404	870	419	272

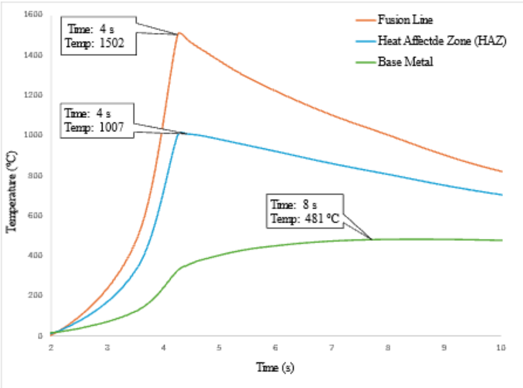

(a)

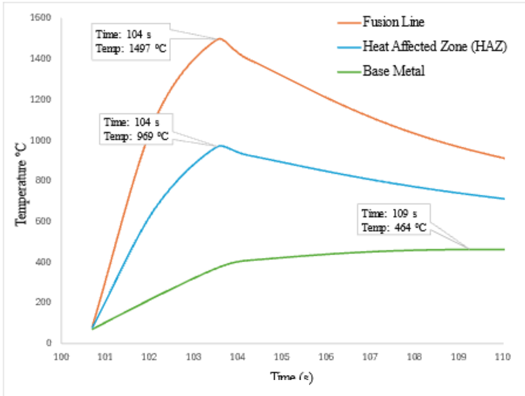

(b)

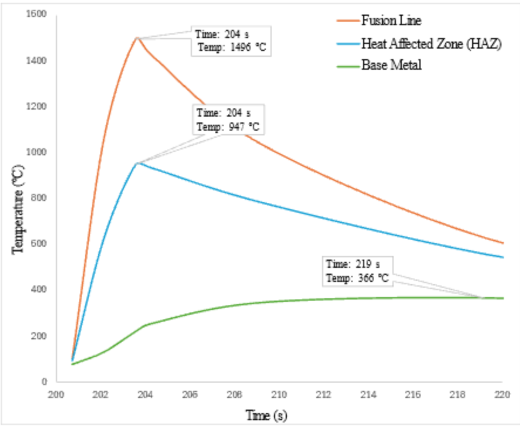

(c)

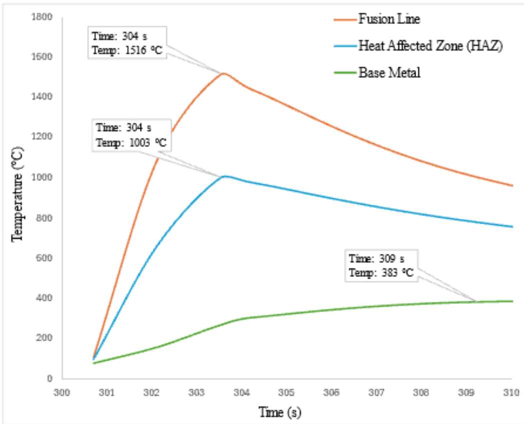

(d)

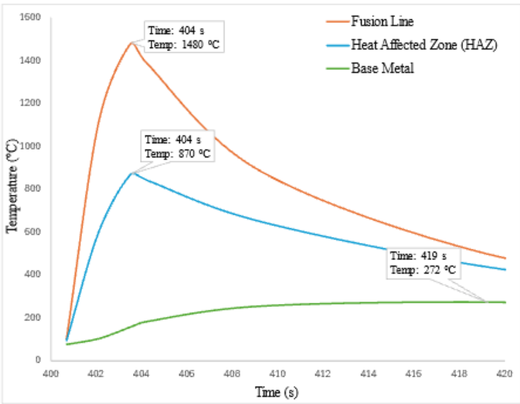

(e)

Figure 14. Zoom-in view of the temperature-time graph of all five passes of model 1, [Graphs from (a to e) are shown the zoom-in view of the temperature profile for (the first, second, third, fourth, and fifth passes, respectively)]

4.1.2 Thermal behaviour analysis of welded regions in model 2

Analysing the temperature profiles for the three welding passes of model 2 using the SAW process in a 21 °C environment reveals insightful information regarding the thermal behaviour of the most important regions in welding process. Therefore, in the study, similar to model 1, the fusion line, HAZ, and base metal zone with specific distance from weld line have been considered for the investigation. Notably, this analysis relies on temperature profiles observed across five welding passes, each followed by a 150 s cooling interval to reach the 42-52 ⁰C interpass temperature to meet the determined interpass temperature in preliminary welding tests results (Figure 15).

In the first pass, initially, the fusion line rapidly attains its highest temperature due to the direct exposure to the welding arc, which is necessary to melt the steel. This temperature peak is promptly followed by a sharp decline, illustrating the significant heat input at the start and the quick cooling that is vital for the weld's solidification. Concurrently, the HAZ reaches a high temperature, although not as high as the fusion line. This reflects the heat diffusing from the weld pool into the surrounding metal, impacting the metal's microstructure and properties. Meanwhile, the base metal heats the least, playing a critical role in absorbing residual heat and facilitating the overall cooling process.

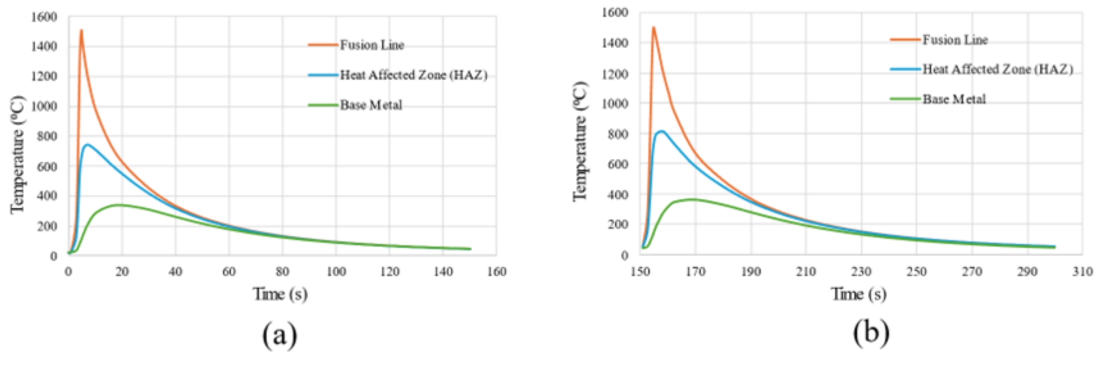

Figure 15. Temperature profiles of three passes of model 2 in the SAW process, [Graphs from (a to c) are shown the temperature profile for (the first, second, and third passes, respectively)]

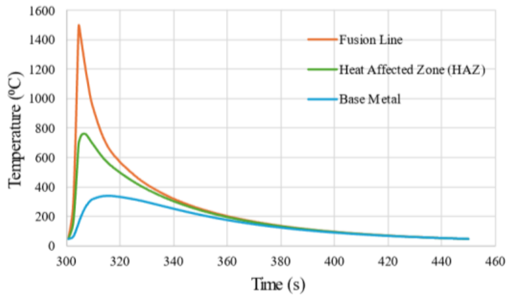

(c)

Figure 15 continues. Temperature profiles of three passes of model 2 in the SAW process, [Graphs from (a to c) are shown the temperature profile for (the first, second, and third passes, respectively)]

Moving into the second and third passes, we observe similar patterns when analysing separately. However, Figure 16 shows the graphs in a zoomed-in view to enable a deeper analysis of the thermal graphs. In comparing these graphs, a few key observations and patterns emerge regarding the behaviour of these three regions.

The peak temperatures for the fusion line are very close across all three passes, with values of 1505 °C at 5 s for the first pass, 1501 °C at 155 s for the second pass, and 1499 °C at 305 s for the third pass. This trend indicates consistent welding heat input across all passes. In HAZ, the peak temperatures show more variation, with the second pass reaching a higher peak temperature of 815 °C at 158 s compared to 744 °C at 7 s for the first pass and 760 °C at 307 s for the third pass. The higher peak temperature in the second pass suggests that this pass introduces more heat into the HAZ, possibly due to the overlapping thermal effects from multiple passes.

For the base metal, the peak temperatures are 335 °C at 18 s for the first pass, 365 °C at 170 s for the second pass, and 343 °C at 316 s for the third pass. The slightly higher temperatures in the second pass reflect cumulative heating effects, indicating that the material retains more heat as subsequent passes are applied. Additionally, by analysing the cooling rates, the fusion line graph shows the fastest cooling in the first pass with a rapid decrease in temperature after the peak. The second and third passes exhibit more gradual cooling due to the pre-heated material from previous passes. In the HAZ, the cooling rates are relatively consistent across all passes but slightly slower in the second pass, corresponding to the higher initial temperatures. Finally, the base metal region exhibits the slowest cooling rates, consistent with its lower peak temperatures. Consequently, the second pass introduces more heat into the material, affecting both the HAZ and the base metal regions more significantly than the first and third passes. This behaviour highlights the cumulative thermal effects of multiple welding passes in the welding process. All the information from Figure 16 are listed in Table 12.

Table 12. Data gathered from temperature-time graphs of model 2

Number of Passes	Fusion line		HAZ		Base Metal	
	Time (s)	Temperature(ºC)	Time (s)	Temperature(ºC)	Time (s)	Temperature(ºC)
NO.1	5	1505	7	744	18	335
NO.2	155	1501	158	815	170	365
NO.3	305	1499	307	760	316	343

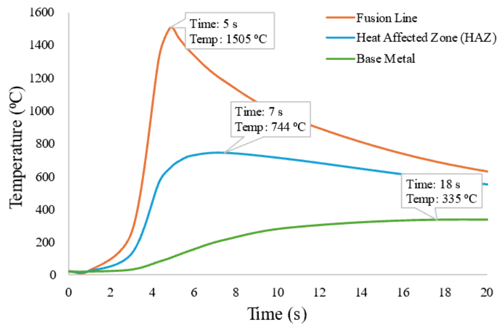

(a)

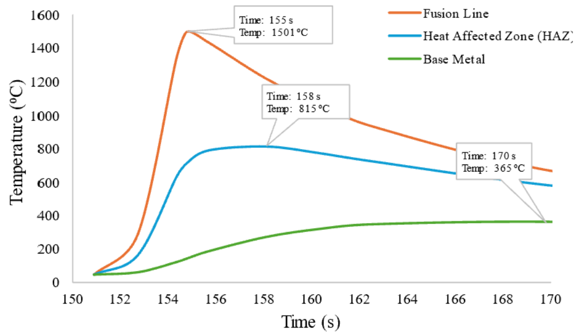

(b)

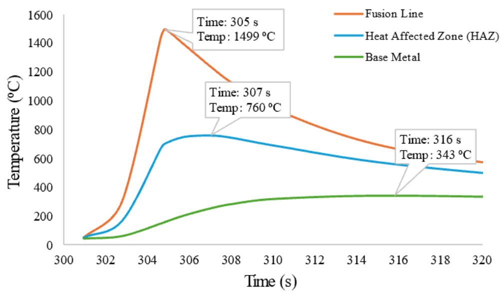

(c)

Figure 16. Zoom-in view of temperature-time graph of three passes of model 2. [Graphs from (a to c) are shown the zoom-in view of the temperature profile for (the first, second, and third passes, respectively)]

4.2 Discussion

The study meticulously examines the thermal behaviour of S700E steel grade under different welding configurations, focusing on the comparative analysis between three-pass and five-pass welded joints. By leveraging advanced thermal simulations through finite element analysis, this research provides a comprehensive understanding of temperature distribution, cooling rates, and thermal gradients during the welding process. These parameters are crucial for predicting microstructural transformations and the resultant mechanical properties of the welded material.

Starting with the fusion line, model 1 reaches its highest peak temperature of 1516.48 °C during the fourth pass, while model 2 achieves a slightly lower maximum of 1505.43 °C in the first pass. This difference indicates that model 1 experiences higher peak temperatures, suggesting a more intense heat input during welding. The highest temperature for model 1 in HAZ is 1007.05 °C during the first pass. In comparison, the HAZ of model 2 peaks in the second pass at 815.30 °C. A more extensive level of thermal exposure is indicated by the higher peak temperature in model 1's HAZ, and this can result in more substantial microstructural changes such grain growth or phase transitions. Model 2's lower peak temperature points to a softer thermal effect that might cause less drastic microstructural transformations. The difference demonstrates how the welding procedure in model 1 exposes the HAZ to higher temperatures, which has a more significant impact on its microstructure than that which occurs on model 2. Furthermore, model 1 reveals a greater initial peak temperature for the base metal on the first pass, 480.81 °C, which progressively drops to 272.00 °C by the fifth pass. On the other hand, the base metal of model 2 reaches its maximum temperature of 365.15 °C during the second pass. The base metal of model 1 has increased temperatures, suggesting an extensive cumulative heat effect that continues heat retention and decreases cooling rates. This continued exposure to heat could promote the development of coarser grains, which could reduce the material's strength and toughness. The lower peak temperatures of Model 2 suggest less intense cumulative heating, which could lead to more homogeneous microstructural features and improved mechanical properties because of rapid cooling rates. Furthermore, an analysis comparing the top pass with the root pass in each model reveals that the root pass consistently achieves a lower maximum temperature across all three regions in both models. This temperature difference is particularly significant in HAZ of Model 1, which the difference is near 130 ºC.

4.3 Comparative thermal behaviour of top passes of model 1 and model 2

In the following, Figure 17 illustrates the thermal behaviour of the top pass for each model, considering the same thermal cycle duration for both models. According to the figure, the fusion line reaches a maximum temperature of about 1500 °C in both models. However, in model 1, the temperature rises to this peak more quickly and then cools down rapidly. This fast thermal cycle means that the heat input in model 1 is more concentrated over a shorter time because of the higher number of passes. Therefore, the fusion line in model 1 heats up and cools down much faster than in model 2. Model 2, that includes a smaller number passes, has a more gradual cooling rate and a partially delayed peak temperature, suggesting a longer-lasting thermal effect. Comparably, Model 1 in the HAZ depicts a sudden increase in temperature to about 1000 °C, which is quickly followed by a catastrophic decrease. This pattern emphasizes the five-pass configuration's strong and short-lived thermal effect. In comparison, model 2 heats up more slowly and cools down gradually over time. It peaks slightly lower, at roughly 800 °C. This variation suggests that model 2's thermal exposure remains constant over a longer time period, leading to less rapid but more persistent heating. Similar behavior is also seen in the base metal region, where model 1 reaches its peak temperature of roughly 380 °C considerably faster than model 2. In model 1, the cooling that occurs afterwards is similarly faster, suggesting that the thermal effect dissipates quickly. Conversely, model 2, with its three-pass structure, heats the base metal more gradually and preserves the temperature higher for a longer time before cooling down gradually. Consequently, the lower heat dissipation in model 2 results in higher temperatures at the end of the cycle for all three regions.

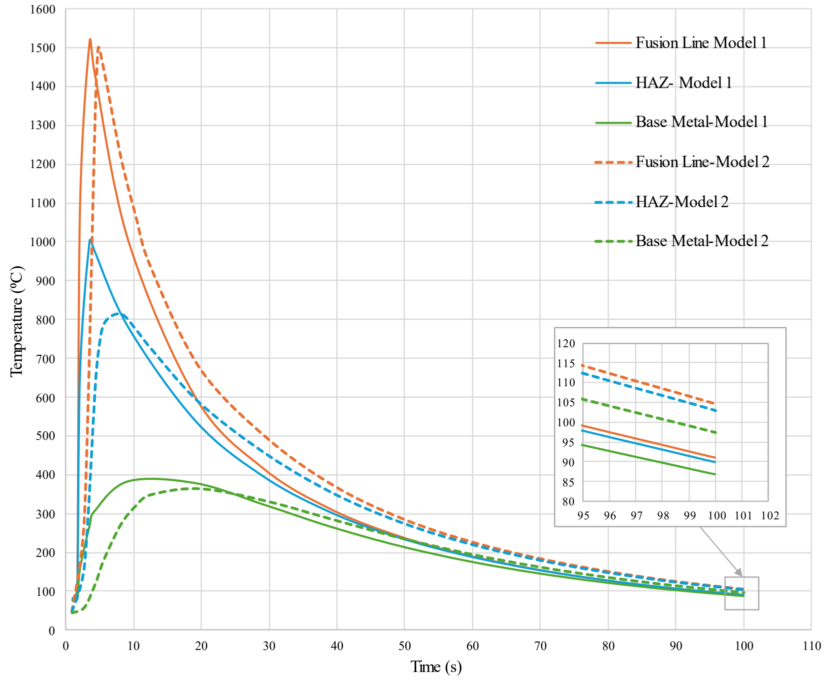

Figure 17. Thermal behaviour of top passes for both model 1 and model 2

4.3.1 Thermal analysis of top passes between 800°c and 500°c

Figure 18 presents the graphs of three regions for both models in the top pass. Analysing the graph, it is evident that model 1 exhibits rapid cooling rates in the fusion line, HAZ, and base metal regions. This evaluation suggests a higher likelihood of forming hard and brittle phases due to the quick temperature drop. The advantage of model 2 lies in its slower cooling rates, which support the development of more ductile microstructures. This slower cooling process reduces the likelihood of internal stresses and brittleness, resulting in a weld with enhanced toughness and crack resistance.

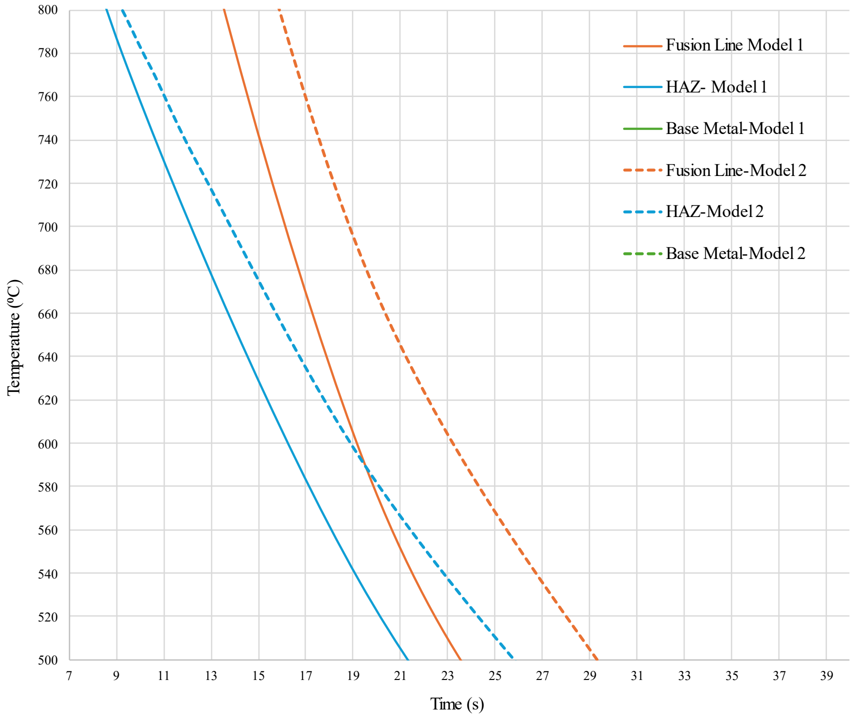

Figure 18. Top pass cooling rates (800 °C-500 °C) for fusion line, HAZ, and base metal regions in Models 1 and 2

4.3.2 CCT diagram

In the following, to determine the influence of the cooling profiles in both models on microstructural development, a careful assessment is considered. After analyzing the cooling rate graphs (Figure 18) against the Continuous Cooling Transformation (CCT) diagram, we can discuss about the cooling rate more confidently. In bellow, Figure 19 demonstrates the cooling behavior of two models for both fusion line and Haz zones. It is evident that the cooling profiles for all four regions in both models promote the development of acicular ferrite. Acicular ferrite is known for its fine, needle-like structure that enhances both the toughness and strength of the steel, making it a desirable phase in welded joints for its positive impact on mechanical properties. Such a uniform transformation across different regions and both models suggests that the welding process has been optimized enough to control the cooling rates adequately, ensuring that the microstructural evolution is beneficial across the entire weld area.

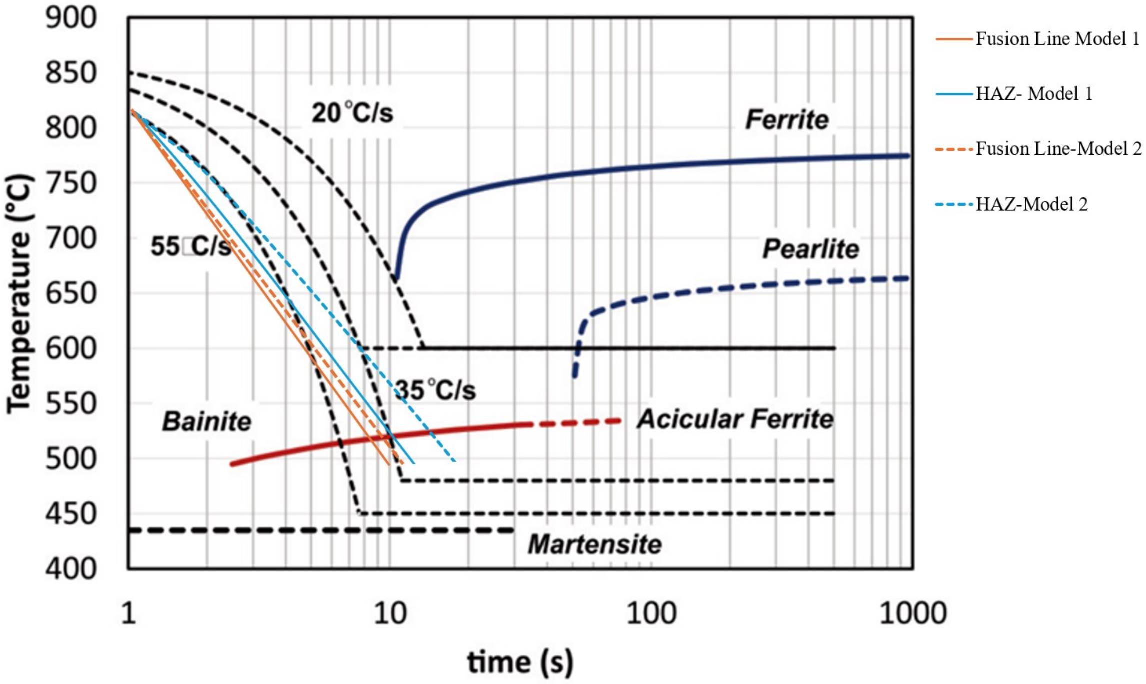

Figure 19. CCT diagram for S700E

5 Conclusion

Numerous important details on the weldability and performance of S700E steel grade configurations under various welding conditions and pass numbers have been discovered by utilizing numerical investigation, specifically in relation to shipbuilding applications. The study emphasized how crucial it is to adjust welding parameters, in order to guarantee the mechanical integrity and highest-quality performance of welded connections. The resilience and dependability of marine structures are greatly dependent on the accurate adaptation of prevalent issues including phase transformations and residual stresses, which can be achieved by carefully controlling these parameters through comprehensive simulations. The results showed that the microstructural alterations inside the weld zone vary significantly depending on the welding configuration and temperature inputs. The toughness, ductility, and resistance to cracking of the welds are among the mechanical characteristics that are directly impacted by these microstructural alterations. The study demonstrated for instance, that slower cooling rates can encourage the formation of more ductile microstructures, minimizing the risk of brittleness and internal stresses and improving the weld's overall quality. Moreover, the investigation yielded a thorough comprehension of the thermal characteristics of S700 steel during the welding procedure. The HAZ's behaviour during multiple welding passes was demonstrated by the simulations, which also displayed variances in peak temperatures and cooling rates. These observations are crucial for forecasting how well welded joints would function in practical settings, especially in the harsh maritime conditions where structural integrity is of the highest priority.

The FEA study offered insightful recommendations for enhancing material selection and welding processes in shipbuilding. The knowledge acquired from this study offers a solution to improve the performance, sustainability, and safety of shipping vessels while also advancing our understanding of the behaviour of S700E steel throughout the welding process.

References

Ban, H. & Shi, G., 2018, ‘A review of research on high-strength steel structures’, Proceedings of the Institution of Civil Engineers: Structures and Buildings. Pp. 30-37

Brätz, O., Arnim, M. von, Eichler, S., Gericke, A., Hildebrand, J., Bergmann, J.P., Kuhlmann, U. & Henkel, K.M., 2023, ‘Mechanical properties of MAG butt welded dissimilar structural steel joints with varying strength from grade S355 up to S960’, Welding in the World, Vol. 67:12. Pp. 1177–1198.

Celin, R., Bernetič, J. & Balantič, D.A.S., 2014, ‘Welding of the steel grade S890QL’, Materiali in Tehnologije. Pp. 1-13.

Chernyshov, E.A., Romanov, A.D. & Romanova, E.A., 2016, ‘High-Strength Shipbuilding Steels and Alloys’, Metallurgist. Pp. 1–2.

Chiew, S.P., Cheng, C., Zhao, M.S., Lee, C.K. & Fung, T.C., 2019, ‘Experimental Study of Welding Effect on S690Q High Strength Steel Butt Joints’, ce/papers. Pp. 3–4.

Dias, J.M.S., Santos Paes, L.E. dos, Santos, A.G.M., Borba, T.M.D., Paixão Carvalho, L. da & Vilarinho, L.O., 2023a, ‘A methodology for multipass gas metal arc welding of shipbuilding steel plates with different thicknesses’, International Journal of Advanced Manufacturing Technology, Vol:127. Pp. 1–2.

Gáspár, M., 2019, ‘Effect of welding heat input on simulated haz areas in s960ql high strength steel’, Metals, Vol:9. Pp. 11-13.

Ghafouri, M., Amraei, M., Pokka, A.P., Björk, T., Larkiola, J., Piili, H. & Zhao, X.L., 2022, 'Mechanical properties of butt-welded ultra-high strength steels at elevated temperatures', Journal of Constructional Steel Research. Pp.83-105.

Ghimire, A., Wald, F., Vild, M. & Kabeláč, J., 2024, 'Numerical design calculation of the high-strength steel welds', Engineering Structures. Pp. 1165-1172.

Górka, J., 2015, 'Weldability of thermomechanically treated steels having a high yield point', Archives of Metallurgy and Materials. Pp. 1-14.

Guo, W., Li, L., Dong, S., Crowther, D. & Thompson, A., 2017, 'Comparison of microstructure and mechanical properties of ultra-narrow gap laser and gas-metal-arc welded S960 high strength steel', Optics and Lasers in Engineering. Pp. 98-122.

Hayat, F. & Uzun, H., 2011, 'Effect of heat treatment on microstructure, mechanical properties and fracture behaviour of ship and dual phase steels', Journal of Iron and Steel Research International. Pp. 8-18.

Hopf, A., Klug, M., Durmaz, K., Goth, K. & Jüttner, S., 2023, 'Introduction of a New Test Methodology for Determining the Delayed Cracking Susceptibility', Journal of Manufacturing and Materials Processing. Pp. 1-7.

Imai, S., 2008, 'Recent progress and future trends for shipbuilding steel', Welding International. Pp. 11-21.

Jiang, J., Wu, M., Xu, T.T., Bao, W. & Li, Z.H., 2024, 'Study on impact toughness of TMCP and quenched and tempered high strength steels', Case Studies in Construction Materials. Pp. 1-25.

Kamo, T., Ando, R., Sasaki, M., Suzuki, T. & Watanabe, Y. Ultra high strength steel for sustainable building structures.2015. 191 p.

Kc, S. & Gautam, D., 2021, Progress in sustainable structural engineering: a review, Innovative Infrastructure Solutions. Pp. 2-6.

Klett, J. & Hassel, T., 2020, ‘Reducing the risk of hydrogen-induced cold cracks in hyperbaric wet welding of high-strength steels by using austenitic welding consumables’, Welding and Cutting. Pp. 1-19.

Kupriyanova, O.A.New Generation High-Strength Cold-Resistant Steels: History, Current Status and Development Prospects: Steel in Translation. 2023. 53 p.

Layus, P., Kah, P., Khlusova, E. & Orlov, V., 2018a, ‘Study of the sensitivity of high-strength cold-resistant shipbuilding steels to thermal cycle of arc welding’, International Journal of Mechanical and Materials Engineering. Pp. 1-13.

Luo, X.D., Liu, H., Zhu, Y.X. & Zheng, C.Y., 2014, Effect of heat treatment on microstructure and mechanical properties of EH36 alloy, Applied Mechanics and Materials. Pp. 487-498.

Moore, P.L. The importance of welding quality in ship construction: Analysis and Design of Marine Structures: Including CD-ROM. 2009. 89 p.

Neuvonen, R., Peltoniemi, T., Skriko, T., Ghafouri, M., Amraei, M., Ahola, A. & Björk, T., 2023a, ‘The effects of geometric and metallurgical constraints on ultra-high strength steel weldments’, Structures. Pp. 56-62.

Pezzato, L., Gennari, C., Chukin, D., Toldo, M., Sella, F., Toniolo, M., Zambon, A., Brunelli, K. & Dabalà, M., 2020, 'Study of the effect of multiple tempering on the impact toughness of forged s690 structural steel', Metals. Pp. 4-10.

Rudskoi, A.I. & Parshin, S.G., 2021, Advanced trends in metallurgy and weldability of high-strength cold-resistant and cryogenic steels, Metals. Pp. 5-12.

Sampath, K., 2021, 'Analysis of a High-Strength Steel SMAW Database', Welding Journal. Pp.12-26.

Schroepfer, D., Witte, J., Kromm, A. & Kannengiesser, T., 2024, 'Stresses in repair welding of high-strength steels—part 1: restraint and cold cracking risk', Welding in the World. Pp. 685-697.

Shahriar Afkhami, 2018, Investigation on the Weldability of Cold-Formed Ultra-High Strength Steels S700MC and S1100. Lappeenranta: February 2024 [Referred 24.02.2024] – master's thesis, LUT University. Available in PDF-file: https://lutpub.lut.fi/handle/10024/157091.

Shekhar, S., Rai, P., Ayub, A., Mata Vaishno, S., Srivastava, A., Sekhar, S., Nema, A., Pandey, A. & Jha, R., 2016, 'Analysis of Welding Joints and Processes', Article in International Journal of Computer Applications. Pp. 34-47.

Siltanen, J., 2023, LASER AND HYBRID WELDING OF HIGH-STRENGTH STRUCTURAL STEELS. Lappeenranta: February 2024 [Referred 24.02.2024]. – PhD thesis, LUT University. 68 p. Available in PDF-file: https://lutpub.lut.fi/handle/10024/165599.

Skowronska, B., Chmielewski, T., Golanski, D. & Szulc, J., 2020, 'Weldability of S700MC steel welded with the hybrid plasma + MAG method', Manufacturing Review. Pp.1-34.

Strenx 700 E/F. 2019. [www- data sheet]. SSAB. 2019. [Referred 28.02.2024]. Available: www.ssab.com.

Preheat/interpass temperatures due to consumable properties. 2024. [www- data sheet]. SSAB, 2024. [Referred 28.02.2024]. Available: www.ssab.com.

Tasalloti, H., Kah, P. & Martikainen, J., 2017, 'Effect of heat input on dissimilar welds of ultra high strength steel and duplex stainless steel: Microstructural and compositional analysis', Materials Characterization. Pp. 123-145.

Wang, D., Zhang, P., Peng, X., Yan, L. & Li, G., 2021, 'Comparison of microstructure and mechanical properties of high strength and toughness ship plate steel'. Pp. 14-19.

Weglowski, M. St. High strength quenched and tempered steels: Weldability and welding', High-Strength Steels: New Trends in Production and Applications. 2018. 256 p.

Węgrzyn, T., Szczucka-Lasota, B., Szymczak, T., Łazarz, B., Cybulko, P. & Jurek, A., 2023, 'Welding of High-Strength Steels for the Automotive Industry'. Pp. 23-34.